Numerical Modeling of the Propagation of an Adiabatic Shear Band

SHINHOU KURIYAMA and MARC ANDRÉ MEYERS

The critical phenomena determining the propagation of an adiabatic shear band occur at its extremity. The stress and strain distributions at the tip of a shear band are calculated as a function of applied shear strain using the finite element method for an elasto-plastic material. Three assumptions simplify the calculations considerably: (a) the mechanical response of the material follows an adiabatic stress-strain curve; (b) the material within the shear band has zero shear strength; (c) the body is taken to be in equilibrium. The distribution of stresses and strains in the adiabatically-deformed material is compared to that of a quasi-statically deformed material. While the stress-strain curve for an isothermally deformed material is monotonic with continuous work-hardening, the adiabatic work-hardening curve reaches a plateau followed by work-softening (due to thermal softening). The stress and strain fields for both cases are nearly identical, except in the region directly in front of the shear band. In the adiabatically-deformed material a thin region ($\sim 5\ \mu m$) with large strains and lowered stresses is produced. This region, in which accelerated deformation takes place as the applied shear deformation increases, is absent in the isothermally-deformed material. The formation of this instability region, ahead of the shear band, is considered to be the mechanism for the propagation of an adiabatic shear band.

I. INTRODUCTION

AN adiabatic shear band is a strain localization phenomenon that occurs when the rate of softening of the material due to temperature increase is greater than the rate of work hardening due to plastic deformation. Adiabatic shear bands have been characterized in numerous metallurgical investigations, and the reviews by Rogers,[1] Bedford *et al.*,[2] and Olson *et al.*[3] attest to this. The mechanical modeling of these bands has also been conducted, with a number of different approaches.[4-16] The work is presented by Mescall and Weiss.[17] The destabilizing effect of thermal softening, reducing the slope of the stress-strain curve in nearly adiabatic deformation, was first recognized by Zener and Hollomon.[9] The nucleation of shear bands was first correlated with the shear strain at which the slope of the adiabatic stress-strain curve is zero by Recht,[4] and this method has been developed further by other researchers.[4,10,11] An elementary linear perturbation analysis of plastic instability due to thermal softening for the nucleation of a shear band was presented by Clifton *et al.*,[12] and this method has been applied by other researchers.[8,13-15] The formation of the shear band was analyzed numerically by Olson *et al.*[3] using the HEMP code (finite difference formulation) and by Lindholm *et al.*,[16] using the EPIC code (finite element method); these codes deal with the combined thermal-mechanical problem. The former analyzed the formation of a shear band produced by the simple shearing in a two-dimensional rectangular body, and the latter analyzed it in a thin-walled tubular specimen subjected to pure torsional loading. A comprehensive development program of a computational model for shear bands has been carried out at SRI-International by Seaman, Curran, Shockey, Erlich, and co-workers.[6,18-20]

SHINHOU KURIYAMA is with Institute of Physical and Chemical Research, Wako, Saitama 351-01, Japan. MARC ANDRÉ MEYERS is with Center for Explosives Technology Research, New Mexico Institute of Mining and Technology, Socorro, NM.

Manuscript submitted June 3, 1985.

In all of these studies, the shear band was treated as an interface (or a region with discrete thickness) of discontinuity.* The present work focuses on the tip of the shear band, and assumes that the critical phenomena dictating the propagation or arrest of a shear band occur at the tip. This approach is analogous to fracture mechanics in which the crack tip is the region where the relevant processes are taking place, while the crack surfaces are merely the product. Indeed, there have been proposals that shear bands are Mode II shear cracks, with friction between the two surfaces at the high strain rates producing welding of the two surfaces (friction welding).

Figure 1 shows the tip of a shear band in AISI 4340 steel in the quenched and tempered condition. The propagation of the shear band takes place by the extension of its right-hand side extremity. The driving energy for the extension of the tip comes from an increase of the imposed displacement d, which generates shear stresses and strains. In the analysis presented in this paper the plastic deformation ahead of a shear band is calculated as a function of deformation (or imposed displacement d).

*Formulations incorporating both heat transfer and the effect of strain rate on the flow stress have been developed by M. Wada, T. Nakamura, and K. Kinoshita (*Phil. Mag. A*, 1978, vol. 38, p. 167), and the effect of strain rate on the flow stress has been developed by M. Wada, T. Nakamura, and K. Kinoshita (*Phil. Mag. A*, 1978, vol. 38, p. 167) and A. M. Merzer (*J. Mech. Phys. Sol.*, 1982, vol. 30, p. 323). G. R. Johnson (*J. Eng. Mat. and Techn.*, 1981, vol. 103, p. 201) compared experimental results with an analysis using the finite element method incorporating strain rate, temperature, and heat transfer effects. However, none of the above analyses addressed the tip of the shear band.

II. MODEL

A. *Assumptions*

A number of assumptions are required to render the problem tractable. The principal assumptions are given and justified below.

(a) *Negligible flow stress in shear band.* Post-deformation measurements have shown that the hardness in the shear band can be very high and often exceeds that of the surrounding material. However, during the process of propagation, plastic deformation is highly localized in the shear-band region, leading to significant temperature increases. Temperatures can approach and possibly exceed the melting point. Assuming adiabaticity, one could calculate the temperature increase as a function of strain; strains as high as 572 have been measured in shear bands.[21] There is evidence that the flow stress in the shear band is much lower than the surrounding material during or immediately following deformation. Rogers[22] (Figure 4, p. 107) shows voids inside a band produced by tension, forming immediately after band formation. These voids are spherical in shape and are restricted to the shear band. He concludes that the band is weaker than surrounding material. Grebe *et al.*[23] (Figure 8, p. 767) observed voids in bands that turn from spherical to elliptical when the void diameter equals the band thickness. Again, the voids restrict themselves to the band, indicating a much lower flow stress inside the band area. Timothy and Hutchings[24] (Figure 5) make the same observation and conclude that "the existence of high temperatures within the shear bands at the end of the loading phase of impact can be inferred indirectly.... from the rounded shapes of the cavities that sometimes form within the shear zones." The only direct measurement of temperature within the shear-band zone is, to the authors' knowledge, the one conducted by Dao and Shockey[25] by an infrared microscope; they found temperatures of 500 °C.

(b) *An adiabatic stress-strain curve represents the plastic deformation process.* Each point in Figure 1, during the band propagation stage, is subjected to a specific strain rate, has a specific temperature, and has a flow stress which depends on the stress, temperature, and previous deformation. An elasto-plastic model which would incorporate these variables and heat transfer would be exceedingly complex. Since plastic deformation is occurring at a high strain rate, the assumption of adiabaticity is a reasonable one. The use of an adiabatic stress-strain equation was introduced by Olson *et al.*[3] and greatly simplifies computer calculations, allowing one single equation to represent the behavior of the material. These stress-strain relationships can be obtained from high-strain-rate torsion or shear tests; the strain rate must be significantly high to assure minimum heat flow and sufficiently low to eliminate plastic wave propagation as a significant contributor. For the model developed in the present paper the adiabatic stress-strain curve for quenched and tempered HY-TUF steel obtained by Olson *et al.*[3] is used; the computational predictions are compared with those of an isothermal material. The use of this adiabatic stress-strain curve allows a realistic modeling by eliminating the need to directly introduce temperature effects; it assumes that the deformation is taking place at the same strain rate throughout the entire specimen.

(c) *The body is assumed to be in quasi-static equilibrium throughout the deformation process.* As such, wave-propagation effects are absent. In order to express the dynamic movement of the body, the stresses are assumed to increase along the adiabatic stress-strain curve (thus, thermal conductivity[26] is not considered) at the high imposed strain rate.

B. *Mechanical Response of Material*

The material is assumed to behave adiabatically. The adiabatic stress-strain curves are characterized by initial work hardening followed by work softening; a plastic

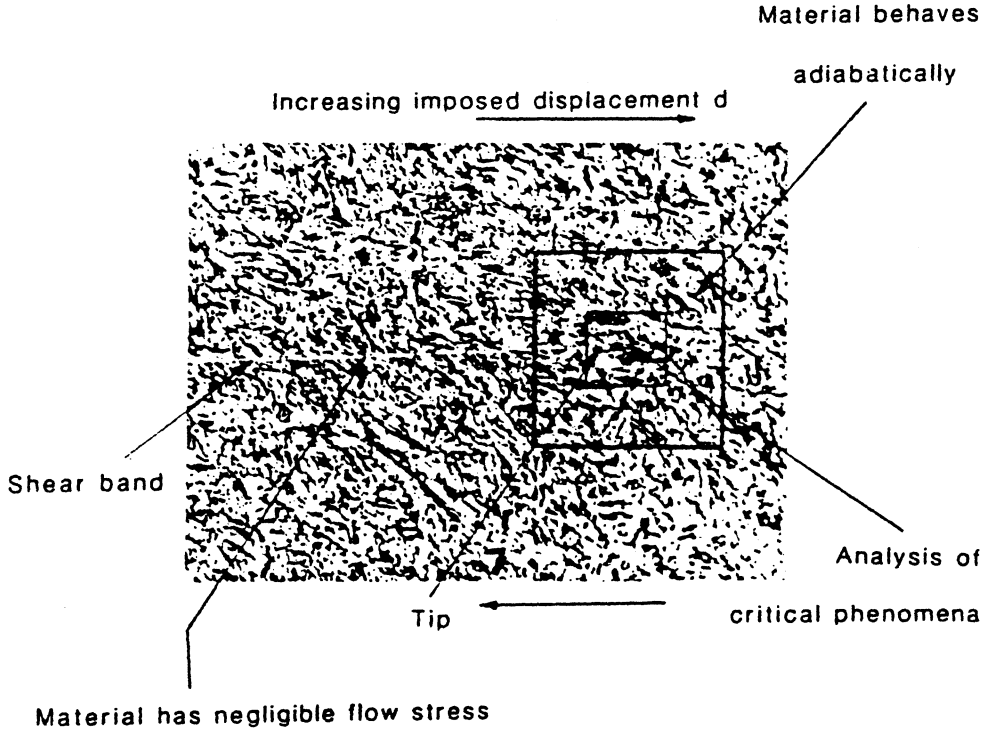

Fig. 1 — Extremity of shear band in AISI 4340 steel in quenched and tempered condition; basic assumptions used in model are indicated (photograph courtesy of C. Wittmar., NMIMT). Magnification 248 times.

instability strain γ_p^i defines the bound between the two regimes. For the model herein developed, the adiabatic stress-strain curve for a high-strength steel determined at a strain rate of $\dot{\gamma} = 10^2\ s^{-1}$ in a torsion test by Olson *et al.*[3] was used. The plastic instability strain γ_p^i is equal to 0.112. This low value establishes some doubt as to whether instability is caused by thermal softening or by some other mechanism, such as subcritical shear microcracks. However, this curve was used for the following reasons: (1) it is one of the few curves available; (2) the computation time for high-strength steel is considerably lower than for low-strength steel, which has an instability strain $\gamma_p^i = 1.11$; (3) the adiabatic stress-strain curve for the same material (HY-TUF in quenched and tempered condition) was used by Olson *et al.*[3] to examine the formation of shear band by simple shearing of an unnotched rectangular body. The following equation was developed by Olson *et al.*[3] to describe the adiabatic shear stress-shear strain curve:

$$\tau = \tau_0(1 + \alpha\gamma_p) \exp(-\beta\gamma_p) \qquad [1]$$

τ is the shear stress and γ_p the plastic shear strain. For the quenched and tempered HY-TUF steel, $\tau_0 = 917$ MPa, $\alpha = 7.85$, and $\beta = 4.18$. The instability strain γ_p^i can be found by setting $d\tau/d\gamma_p^i$ equal to zero. One finds that $\tau_{max} = 1079$ MPa and $\gamma_p^i = 0.112$. Converting Eq. [1] into effective stress *vs* effective strain:[26]

$$\bar{\sigma} = \bar{\sigma}_0(1 + \alpha\bar{\varepsilon}_p) \exp(-\beta\bar{\varepsilon}_p) \qquad [2]$$

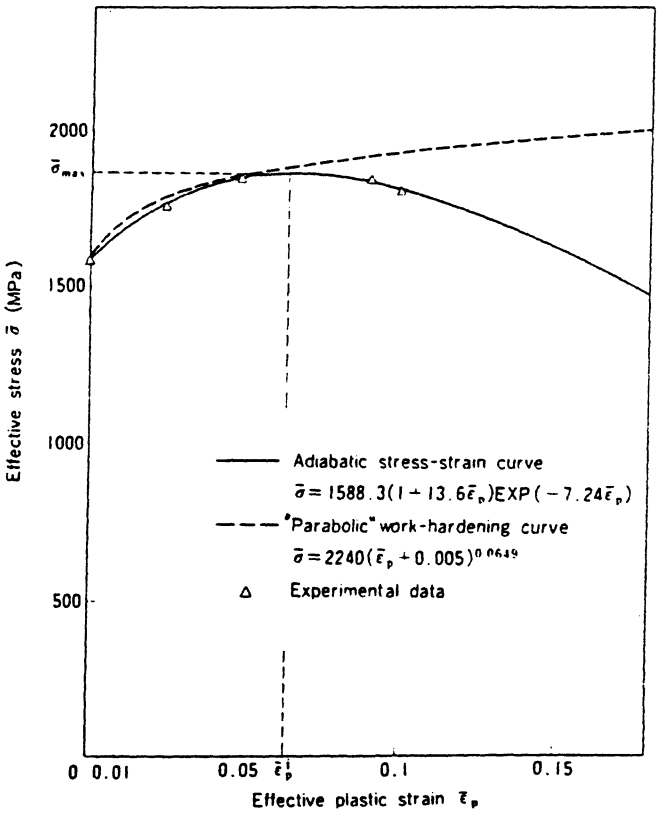

Fig. 2—Effective stress-strain curves for HY-TUF steel in quenched and tempered condition. Full line indicates adiabatic behavior, representative of high-strain-rate deformation; dashed curve represents monotonic work-hardening curve, representative of low-strain-rate deformation (data from Olson *et al.*[3]).

where $\bar{\sigma}_0 = 1588.3$ MPa, $\alpha = 13.6$, $\beta = 7.24$, $\bar{\varepsilon}_p^i = 0.0646$, and $\bar{\sigma}_{max} = 1868.9$ MPa. The material constants for elastic deformation are $E = 206.7$ GPa (Young's modulus) and $\nu = 0.28$ (Poisson's ratio). The adiabatic effective stress–effective strain curve is shown in Figure 2 by a solid line.

In order to compare the propagation of the shear band under an adiabatic condition with the progressive deformation produced under conditions where no instability occurs, a "parabolic" work hardening curve shown by the broken line (Figure 2) was developed. It simulates the isothermal behavior of the material, if the assumption that instability is generated by thermal softening is a correct one. Up to the instability strain γ_p^i it is very close to the adiabatic curve. Beyond instability, the two curves diverge markedly, with the "parabolic" curve being represented by:

$$\bar{\sigma} = 2240(\bar{\varepsilon}_p + 0.005)^{0.0649} \qquad [3]$$

C. *Computational Method*

The assumptions enumerated in Section II-A allow the problem to be modeled by the finite-element method for an elasto-plastic material. The mechanical behavior of the material is assumed to obey the von Mises flow criterion and the incremental theory of Prandtl-Reuss.[26] Deformation of the rectangular body is treated as a plane-strain problem where displacements are given as the boundary condition. The form of elements is triangular, and the displacement function is expressed by a linear polynomial. The adiabatic stress-strain curve given by Eq. [2] is used as a constitutive equation in the present code.[27-30]

An element stiffness matrix $[K]$, expressed per unit thickness, is given by

$$[K] = \Delta[T^{-1}]^T[B]^T[D][B][T^{-1}] \qquad [4]$$

where Δ is the area of a triangular element, $[B][T^{-1}]$ is the matrix between the strains and the nodal displacements of the element, and $[D]$ is stress-strain matrix. The matrix $[D]$ is represented by

$$[D] = \frac{E}{(1+\nu)(1-2\nu)}\begin{bmatrix} 1-\nu & \nu & 0 \\ \nu & 1-\nu & 0 \\ 0 & 0 & (1-2\nu)/2 \end{bmatrix} - \gamma\frac{2G}{S_0}\begin{bmatrix} \sigma_x'^2 & \sigma_x'\sigma_y' & \sigma_x'\tau_{xy} \\ \sigma_x'\sigma_y' & \sigma_y'^2 & \sigma_y'\tau_{xy} \\ \sigma_x'\tau_{xy} & \sigma_y'\tau_{xy} & \tau_{xy}^2 \end{bmatrix} \qquad [5]$$

where $S_0 = 2\bar{\sigma}^2H/(9G) + 2\bar{\sigma}^2/3$. γ is taken as 0 when an element deforms elastically, and taken as 1 when the element deforms elasto-plastically. E is Young's modulus, G is the shear modulus, ν is Poisson's ratio, σ_x' and σ_y' are the deviatoric stresses, and $\bar{\sigma}$ and $\bar{\varepsilon}_p$ are the effective stress and effective plastic strain, respectively.

H, the rate of strain-hardening, has been defined by $H = d\bar{\sigma}/d\bar{\varepsilon}_p$ obtained from a conventional stress-strain curve.[29] However, the values of $\bar{\sigma}^*$ and $\bar{\varepsilon}_p^*$ in the process of calculation always deviate from the theoretical stress-strain curve $(\bar{\sigma}, \bar{\varepsilon}_p)$ given by Eq. [2] or [4]. Therefore, the rate is defined as $H = (\bar{\sigma} - \bar{\sigma}^*)/(\bar{\varepsilon}_p - \bar{\varepsilon}_p^*)$ where $\bar{\varepsilon}_p = \bar{\varepsilon}_p^* + \Delta\bar{\varepsilon}_p$ in the present FEM code, which has been modified from Swedlow's code.[27] $\Delta\bar{\varepsilon}_p$ is given as an input datum of

an incremental plastic strain for determining the rate H. This definition suppresses the divergence of calculations automatically. The Gauss elimination method is used for obtaining the incremental displacements of nodal points from a structural stiffness matrix assembled by using all the element matrices.

D. *Mesh and Boundary Conditions*

Metallographic observations indicate that the band thickness, in steels, is in the range 1 to 30 μm. In the model developed herein the band width was assumed to have a thickness of 20 μm. The material within the band is assumed to have zero strength; the extremity of the band is taken to be approximately semi-circular. Figure 3(a) shows the mesh used to analyze the stresses and strains in the extremity of the shear band. The shape is a rectangle with a width of 400 μm and a length of 500 μm. The shear band is represented by a notch with a semi-circular extremity with a 10 μm radius (BAB') in Figure 3(a); the notch has a depth of 60 μm and a width of 20 μm. The mesh contains 318 elements and 176 nodal points.

In spite of the dynamic nature of the propagation of shear bands, the rate of change of stresses is assumed to be sufficiently low to allow for equilibration. Stress waves produced by impact travel up and return down repeatedly along the y-direction between CD and C'D', leading to equilibration after a few reflections. The deformation of the notched body is considered to approach asymptotically the deformation produced by simple shearing in quasi-static equilibrium. Therefore, the tangential displacements are applied on the boundary CD in the x-direction and on the boundary C'D' in the opposite direction, these boundaries in y-direction being fixed. The shear band is considered to propagate into an infinite material in the x-direction, so that the displacements in x-direction given along a boundary DED' vary linearly as shown in the Figure 3(b) and its boundary condition in y-direction is fixed.

The mesh division of Figure 3(c) is used for solving the stress and strain distribution around the tip of the band in detail. The shape is rectangular, with a width of 30 μm and a length of 60 μm. This rectangle is also indicated by a thicker line in Figure 3(a). Displacements obtained along G'H', H'I', I'J', and J'G' in Figure 3(a) are applied to the mesh division of Figure 3(c), which contains 288 elements and 169 nodal points. The area G'H'I'J' in Figure 3(a) contains only 36 elements; hence, the number of elements was increased eight-fold.

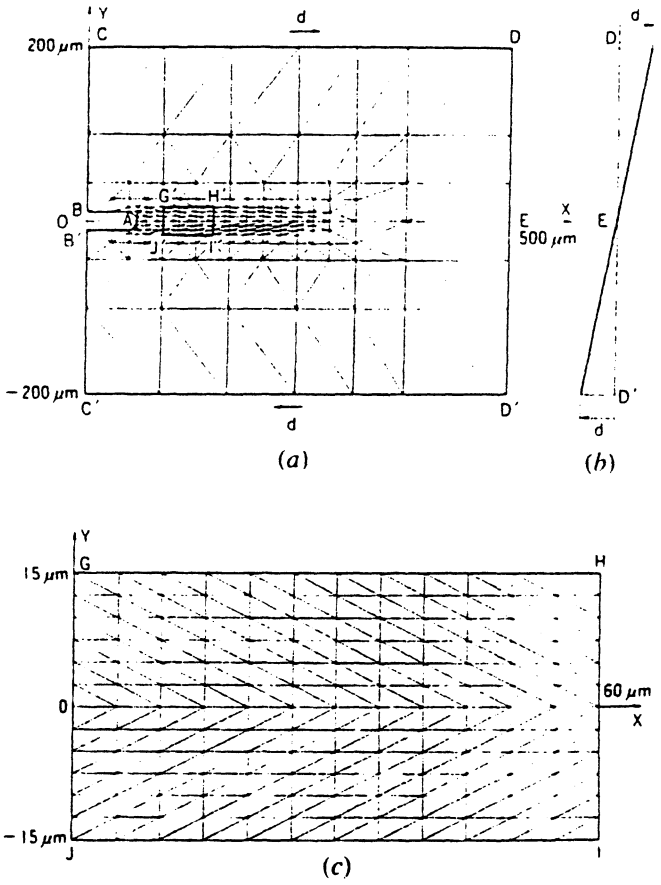

Fig. 3—Mesh divisions used for simple shear deformation: (*a*) notch in a rectangular body; (*b*) boundary displacements imposed along boundary DED'; (*c*) mesh used for obtaining detailed stress and strain distribution around tip of notch.

III. MODEL PREDICTIONS

The model represented by the mesh shown in Figure 3(a) simulates two situations: (a) the initiation of shear-band formation (by simple shear deformation) at the tip of a notch; (b) the propagation of a shear band, assuming that the region within the band and close to its tip has zero shear strength. A simple shear deformation is thus applied to the rectangular body of Figure 3(a); its elasto-plastic response is assumed to obey the adiabatic effective stress–effective strain behavior represented by Eq. [2] with the parameters $\bar{\sigma}_0$, α, and β specified for the quench-and-tempered HY-TUF steel. Figure 4(a) shows the deformed grid after a tangential displacement d = 6.87 μm is given. The lighter boundary lines show the initial rectangle. The isostress (and, consequently, isostrain) contour lines are shown in Figure 4(b). The stresses and strains marked along the lines are effective values. It can be seen that, although the stress level is fairly high in the whole body (1588 to 1869 MPa), the plastic strain is concentrated on a narrow band ahead of the notch tip. No plastic deformation occurs at the corners B and B', because they are part of free surfaces. Uniform plastic deformation is produced near the boundary DED', because effects of the free surface CC' and of the stress concentration at the notch tip do not disturb the stress and strain distribution near the boundary DED'.

A thicker solid curve in Figure 4(b) shows a contour line of $\bar{\sigma}$ = 1869 MPa and $\bar{\varepsilon}_p$ = 0.0646; these values correspond to the maximum stress $\bar{\sigma}_{max}$ and the instability strain $\bar{\varepsilon}_p^i$ at the transition point on the adiabatic stress-strain curve. The stress outside the contour line shown by the solid curve increases with increasing plastic strain due to strain-hardening; however, the stress inside the contour line decreases with increasing plastic strain due to strain-softening. This behavior is shown explicitly in Figure 5(a), where the distributions of stress and plastic strain are shown only in the vicinity of the notch tip. The region contained within the isostress line ($\bar{\sigma}$ = 1869 MPa) is considered to correspond to the shear band. The tip of the contour line of the

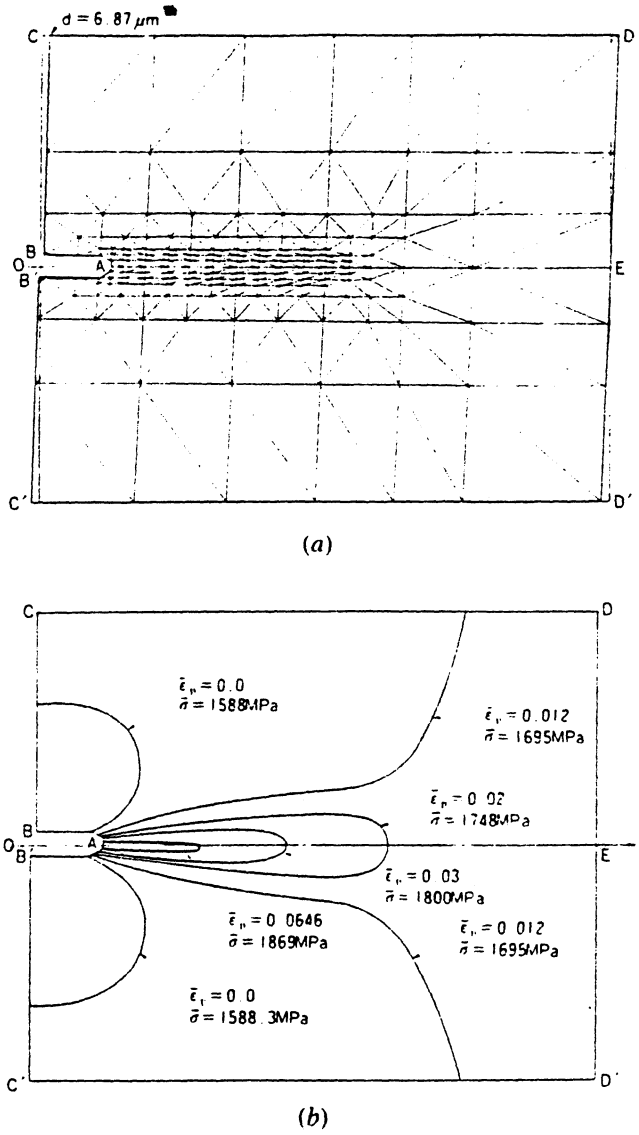

Fig. 4—(*a*) Deformation of the notched body produced by tangential displacement of d = 6.87 μm. Rectangular body before and after the deformation shown by thin and thick solid lines, respectively. (*b*) Isostress ($\bar{\sigma}$) and isostrain ($\bar{\varepsilon}_p$) contour lines in material with adiabatic stress-strain curve. Shear band is produced in narrow zone surrounded by a solid curve, whose values of stress and plastic strain correspond to maximum stress $\bar{\sigma}_{max}$ (1869 MPa) and instability strain $\bar{\varepsilon}_p'$ (0.0646) on the adiabatic curve.

shear band reaches a distance of 80 μm from the notch tip when the tangential displacement is 6.87 μm. The shear band propagates straight along the notch direction, deviating only slightly from the symmetry line OE.

In order to compare the propagation of a shear band with the progressive deformation produced in a material which has no instability region, the deformation of the notched body is determined for the monotonic work-hardening curve, represented by Eq. [3]. Figure 5(b) shows the distribution of effective stress and plastic strain near the notch in the parabolic work-hardening material. The deformation of the body and the distributions of stress and strain are almost the same with those in the material of the adiabatic curve except in the vicinity of the notch tip. The isostrain line for $\bar{\varepsilon}_p$ = 0.0646 is shown by a solid curve in Figure 5(b); this value is equal to the instability strain $\bar{\varepsilon}_p'$ of the adiabatic curve. The stress inside the contour line shown by the solid curve increases with increasing plastic strain. This behavior is the same as that outside the contour, but opposite to that of the adiabatic curve. This contour line reaches a distance of 50 μm from the notch tip when the tangential displacement is 6.87 μm. This deformation progresses exactly on the line OE as shown in the Figure 5(b), compared with the propagation of shear band shown by a broken line. The concentration of strain within the $\bar{\varepsilon}_p$ = 0.0646 isostrain line, with the attendant reduction of stress, is the critical feature responsible for the propagation of a shear band. By increasing the imposed displacement d, this behavior becomes more and more pronounced; the stress within the instability strain contour line will decrease as d is increased. This drastic difference between adiabatic and isothermal deformation within the $\bar{\varepsilon}_p'$ = 0.0646 envelope contrasts with the nearly identical isostress and isostrain contours outside the envelope. This shows that the overall stress distribution is very similar and explains the *localization* of the shear along a narrow band. In Figure 5(b), the width of the $\bar{\varepsilon}_p'$ = 0.0646 envelope is of approximately 10 μm.

In order to assess more clearly the effect of the increasing tangential displacement d on the plastic strain distribution along the symmetry axis OE (Figure 4(a)), the plots shown in Figure 6 and 7 were made. The symmetry axis OE is indicated by X'X' in Figure 6. The effective plastic strain $\bar{\varepsilon}_p$ is plotted as a function of distance along X'X' in Figure 6. Since the notch has a length of 60 μm, the origin is set at 60 μm. The dashed lines represent the isothermal (work-hardening) behavior, while the full lines indicate the adiabatic behavior. At imposed displacements below 3.60 μm, the two conditions deform identically. As d is increased, the plastic shear strain increases at a faster rate for the adiabatic than for the isothermal curve. The difference is highest at the notch tip. In order to see more clearly this difference, the displacements along the Y'Y' axis, passing through the element directly on the tip of the notch, are plotted in Figure 7. The plastic strain $\bar{\varepsilon}_p$ at the node closest to tip of the notch is shown in Figure 8(a); both nodes 130 and 160 have the same strain. They are shown in the left-hand side of Figure 8(a). The data of Figure 8 show the same very clear differences between the two cases when $\bar{\varepsilon}_p'$ is exceeded. While the plastic strain increases linearly with the tangential displacement for the isothermal curve, in the adiabatic curve there is a marked increase in the rate of change of $\bar{\varepsilon}_p$, when $\bar{\varepsilon}_p'$ is exceeded. The length of the instability region is indicated as S in Figure 8(b). This region is defined as the length of the $\bar{\varepsilon}_p$ = 0.0646 envelope for purposes of comparison with the work-hardening curve. Again, the lengths S show marked differences for the two cases beyond a critical displacement d. The length of the instability region S increases very rapidly with increasing displacement d for the adiabatic behavior.

Attempts were made at increasing the displacement d further, but serious problems arose regarding the divergence of the solution. Therefore, it was not possible to analyze the full range of the adiabatic stress-strain curve. However, the trends shown in Figures 4 through 8 can only accentuate themselves as displacement d is increased.

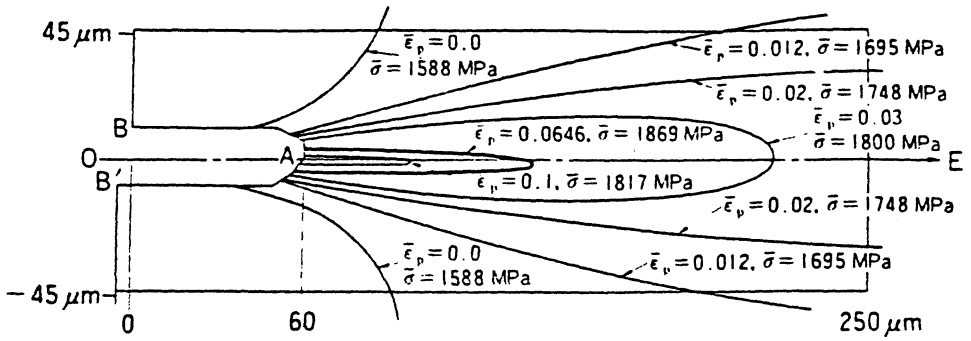

(*a*)

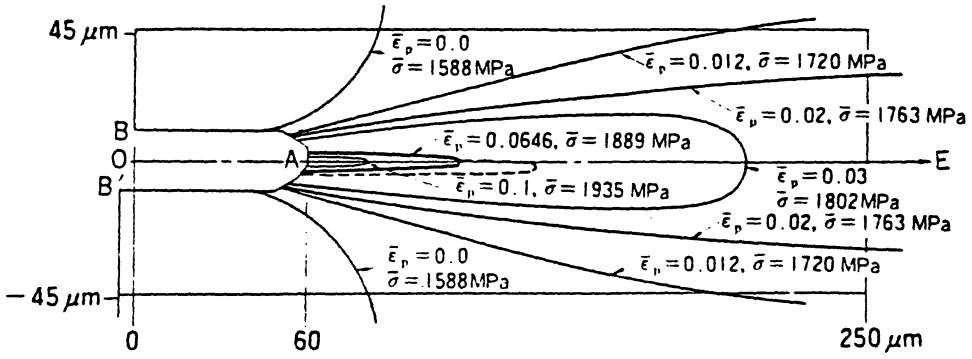

(*b*)

Fig. 5—(*a*) Isostress ($\bar{\sigma}$) and isostrain ($\bar{\varepsilon}_p$) contour lines near the notch in material with adiabatic stress-strain curve. Shear band is produced inside an envelope of solid line $\bar{\varepsilon}_p = 0.0646$. (*b*) Isostress ($\bar{\sigma}$) and isostrain ($\bar{\varepsilon}_p$) contour lines near the notch in material with work-hardening curve.

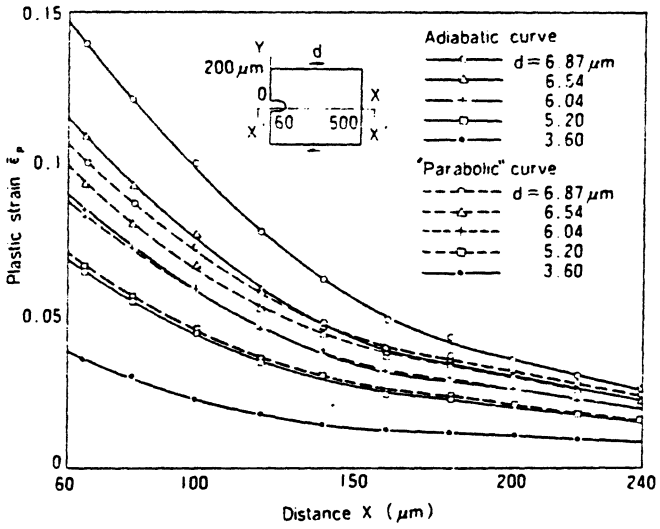

Fig. 6—Comparison of plastic strain distributions along X′X″ between material with adiabatic stress-strain curve and material with monotonic work-hardening curve.

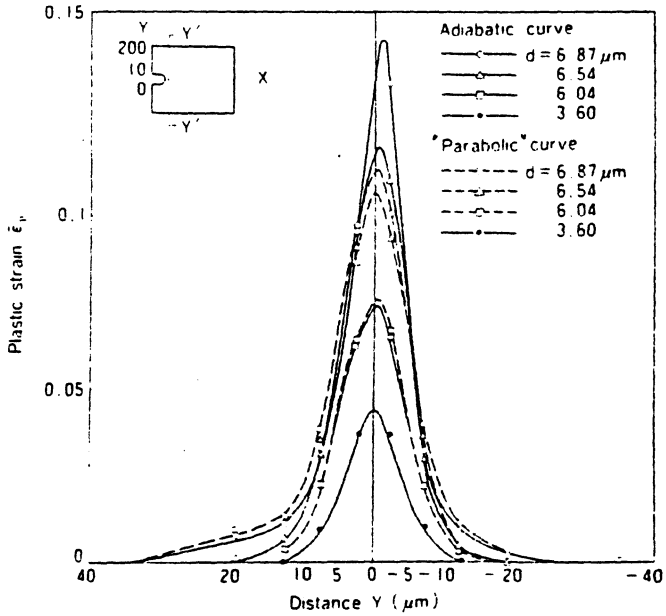

Fig. 7—Comparison of plastic strain distributions along Y′Y″ between a material with adiabatic stress-strain curve and with monotonic work-hardening curve.

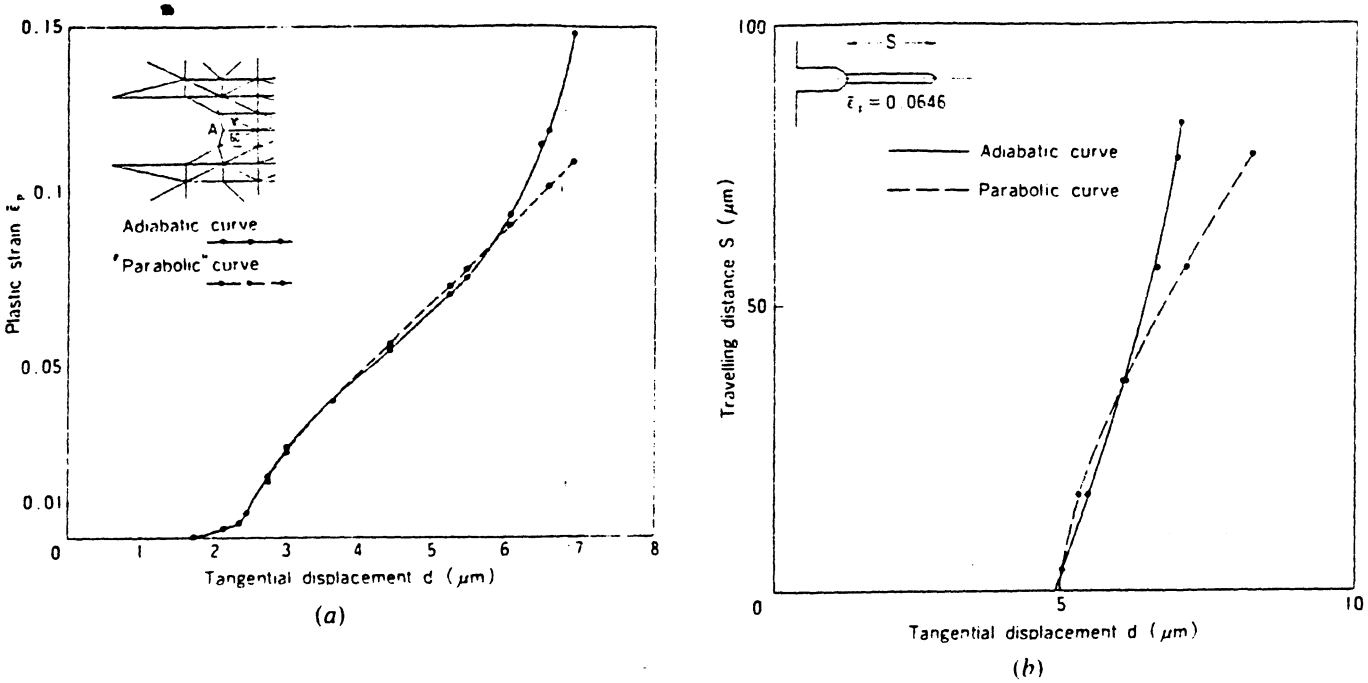

Fig. 8 — (*a*) Plastic strain $\bar{\epsilon}_p$ in an element 160 as a function of tangential displacement *d* for both adiabatic and monotonic work hardening curves. (*b*) Length of shear band for adiabatic stress-strain curve compared with corresponding distance *S* for monotonic work-hardening curve.

IV. CONCLUSIONS

The formation of an adiabatic shear band takes place by the extension of its tip. The high strain rates, at which this phenomenon usually takes place, are required for the production of thermal softening. The finite element method incorporating both elastic and plastic response of the material is used successfully to determine the stresses and strains surrounding a shear-band tip as a function of increased applied shear strain. Three important assumptions are used in order to render the problem mathematically tractable: (a) the material within the shear band is assumed to have negligible shear strength, due to thermal softening; (b) an adiabatic stress-strain curve represents the material behavior; (c) no wave-propagation effects are considered. The data used are taken from Olson *et al.*[3] for a HY-TUF steel showing a work-softening region following work hardening. The results show that the stress fields for an adiabatically and isothermally (monotonic work hardening) deformed material are essentially identical, except in the region directly ahead of the shear-band tip. For the adiabatically-deformed material, a band of material with accelerated deformation ahead of the shear band forms. This region corresponds to the portion of the stress-strain curve where work softening sets in. As the strain increases, the stress decreases in that region. In effect, increasing imposed shear deformation will gradually reduce the stress in that region, until it can be considered part of the shear band. As this happens, the stress fields ahead of the band continuously change to produce this strain-concentration region. For the monotonic work-hardening material such a concentration of stress/strain is not present because work hardening renders deformation at the band tip more and more difficult.

ACKNOWLEDGMENTS

This work was carried out at New Mexico Institute of Mining and Technology. The authors wish to thank Mr. H. A. Grebe (NMIMT), Dr. Han-ryong Pak (NMIMT), and Mr. K. Miyauchi (The Institue of Physical and Chemical Research, Japan) for valuable discussions, and Dr. J. L. Swedlow (Carnegie-Mellon University) for permission to use the code. This research was supported by NSF Grant 8115127 and by the Center for Explosives Technology Research.

REFERENCES

1. H. C. Rogers: *Ann. Rev. Matls. Sci.*, 1979, vol. 9, pp. 283-311.
2. A. J. Bedford, A. L. Wingrove, and K. R. L. Thompson: *J. of the Austr. Inst. of Metals*, 1974, vol. 19, pp. 61-73.
3. G. B. Olson, J. F. Mescall, and M. Azrin: in *Shock Waves and High-Strain-Rate Phenomena in Metals*, M. A. Meyers and L. E. Murr, eds., Plenum Press, New York, NY, 1981, pp. 221-47
4. R. F. Recht: *J. Appl. Mech. (Trans. A.S.M.E.)*, 1964, vol. 31, pp. 189-93.
5. R. S. Culver: in *Metallurgical Effects at High Strain Rates*, R. W. Rohde, B. M. Butcher, J. R. Holland, and C. H. Karnes, eds., Plenum Press, New York, NY, 1973, pp. 519-30.
6. D. C. Erlich, D. R. Curran, and L. Seaman: "Further Development of a Computational Shear and Model," Report AMMRC TR 80-3, SRI-International, Menlo Park, CA, 1980.
7. R. F. Clifton: in *Materials Response to Ultra-High Loading Rates*, W. Herrmann, ed., MMAB-356, National Academy of Sciences, Washington, DC, 1980, p. 129.
8. Y. L. Bai: in source cited in Ref. 3, pp. 277-84.
9. C. Zener and J. H. Hollomon: *J. Appl. Phys.*, 1944, vol. 15, pp. 22-32.
10. A. S. Argon: in *The Inhomogeneity of Plastic Deformation*, ASM, Metals Park, OH, 1973, pp. 161-89.
11. M. R. Staker: *Acta Metall.*, 1981, vol. 29, pp. 683-89.

12. R. F. Clifton, J. Duffy, K. A. Hartley, and T. G. Shauki: *Scripta Met.*, 1984, vol. 18, pp. 443-48.
13. L. S. Costin, E. E. Crisman, R. H. Hanley, and J. Duffy: in *Second Conf. on the Behavior of Materials at High Rates of Strain*, Oxford, England, 1979, pp. 90-100.
14. T. J. Burns and T. G. Trucano: *Mechanics of Materials*, 1982, vol. 1, pp. 313-24.
15. D. E. Grady: *J. Geophys. Res.*, 1980, vol. 85, pp. 913-24.
16. U. S. Lindholm, A. Nagy, G. R. Johnson, and J. M. Hogfeld: *J. Eng. Matls. and Techn.*, 1980, vol. 102, pp. 376-81.
17. *Material Behavior Under High Stress and Ultrahigh Loading Rates*, J. Mescall and V. Weiss, eds., Plenum, New York, NY, 1983.
18. D. C. Erlich, L. Seaman, D. A. Shockey, and D. R. Curran: "Development and Application of a Computational Shear Band Model," Contract Report ARBL-CR-00416, SRI-International, Menlo Park, CA, March 1980.
19. D. R. Curran: Computational Model for Armor Penetration, Contract DAAK11-78-C-0115, Report PYU 7893, SRI-International, Menlo Park, CA, November 1979.
20. D. C. Erlich, L. Seaman, T. Cooper, R. D. Caligiuri, and D. R. Curran: Computational Model for Armor Penetration, Contract DAAK11-78-0115, Report PYU 7853, SRI-International, Menlo Park, CA, April 1983.
21. G. L. Moss: in source cited in Ref. 3, pp. 299-312.
22. H. C. Rogers: in *Material Behavior under High Stress and Ultrahigh Loading Rates*, J. Mescall and V. Weiss, eds., Plenum, New York, NY, 1983, pp. 101-08 (Fig. 4, p. 107).
23. H. A. Grebe, H-r. Pak, and M. A. Meyers: *Metall. Trans. A*, 1985, vol. 16A, pp. 761-75 (Fig. 8, p. 767).
24. S. P. Timothy and I. M. Hutchings: *Acta Metall.*, 1985, vol. 33, pp. 667-70.
25. K. C. Dao and D. A. Shockey: *J. Appl. Phys.*, 1979, vol. 50, pp. 8244-46.
26. W. Johnson and P. B. Mellor: *Plasticity for Mechanical Engineers*, D. Van Nostrand, New York, NY, 1962.
27. J. L. Swedlow: *Computers and Structures*, 1973, vol. 3, pp. 879-98.
28. S. Kuriyama, H. Hayashi, and S. Yoshida: in *Proceedings of the 4th International Conference on Production Engineering*, Tokyo, Japan, 1980, p. 38.
29. Y. Yamada: *Applications of the Finite Element Method*, Univ. of Tokyo, Tokyo, Japan, 1972, pp. 149, 315 (in Japanese).
30. O. E. Zienkiewicz: *The Finite Method in Engineering Science*, 2nd ed., McGraw-Hill, London, England, p. 50.